10-15-2022

# Abnormal vestibular brainstem structure and function in an animal model of autism spectrum disorder

Yusra Mansour
*Henry Ford Health*, ymansou1@hfhs.org

Alyson Burchell

Randy Kulesza



## Recommended Citation
Mansour Y, Burchell A, and Kulesza R. Abnormal vestibular brainstem structure and function in an animal model of autism spectrum disorder. Brain Res 2022; 1793:148056.

Brain Research 1793 (2022) 148056

Contents lists available at ScienceDirect

Brain Research

journal homepage: www.elsevier.com/locate/brainres

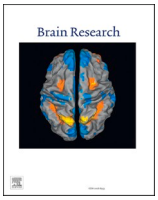

# Abnormal vestibular brainstem structure and function in an animal model of autism spectrum disorder

Yusra Mansour [a,b], Alyson Burchell [a], Randy Kulesza [a,*]

[a] Department of Anatomy, Lake Erie College of Osteopathic Medicine, Erie, PA, United States
[b] Henry Ford Macomb Hospital, Department of Otolaryngology – Head and Neck Surgery, Clinton Township, MI, United States

ARTICLE INFO

*Keywords:*
Development
Inner ear
Cerebellum
Ataxia

ABSTRACT

Autism spectrum disorder (ASD) is a neurodevelopmental disorder that includes several key neuropathological changes and behavioral impairments. *In utero* exposure to the anti-epileptic valproic acid (VPA) increases risk of an ASD diagnosis in human subjects and timed *in utero* exposure to VPA is a clinically relevant animal model of ASD. Many human subjects with ASD have cerebellar hypoplasia, fewer Purkinje cells, difficulties with balance, ophthalmic dysfunction and abnormal responses to vestibular stimulation and such vestibular difficulties are likely under reported in ASD. We have recently shown that animals exposed to VPA *in utero* have fewer neurons in their auditory brainstem, reduced axonal projections to the auditory midbrain and thalamus, reduced expression of the calcium binding protein calbindin (CB) in the brainstem and cerebellum, smaller and occasionally ectopic cerebellar Purkinje cells and ataxia on several motor tasks. Based on these findings, we hypothesized that *in utero* VPA exposure similarly impacts structure and function of the vestibular brainstem. We investigated this hypothesis using quantitative morphometric analyses, immunohistochemistry for CB, a battery of vestibular challenges, recording of vestibular-evoked myogenic potentials and spontaneous eye movements. Our results indicate that VPA exposure results in fewer neurons in the vestibular nuclei, fewer CB-positive puncta, difficulty on certain motor tasks, longer latency VEMPs and significantly more horizontal eye movements. These findings indicate that the vestibular nuclei are impacted by *in utero* VPA exposure and provide a basis for further study of vestibular circuits in human cases of ASD.

## 1. Introduction

Autism spectrum disorder (ASD) is a neurodevelopmental condition characterized by neuropathological changes and impairments in social, communicative and behavioral domains (Allen, 1988; Wing, 1997; APA, 2013; Smith et al., 2019; Mansour et al., 2021; CDC.gov, 2022). Approximately 1 in 44 children are diagnosed with ASD and males are diagnosed four times more frequently than females (CDC.gov, 2022). Beyond well documented behavioral characteristics, the majority of subjects with ASD demonstrate some degree of auditory and vestibular dysfunction (reviewed in Mansour et al., 2021). Consistent with these functional impairments, neuropathological changes in the brainstem and cerebellum of human subjects with ASD are well documented (Ornitz, 1969; Courchesne et al., 1988; Hasimoto et al., 1992; 1995; reviewed in Smith et al., 2019).

*In utero* exposure to the antiepileptic valproic acid (VPA) significantly increases risk of ASD in human subjects (Moore et al. 2000; Williams et al. 2001; Rasalam et al. 2005; Koren et al. 2006; Bromley et al. 2013; Christensen et al. 2013). Accordingly, timed *in utero* exposure to VPA is a biologically relevant and validated animal model of ASD (rodents: Rodier et al., 1996; Mabunga et al., 2015; primates: Zhao et al., 2019). In fact, many of the morphological changes identified in the auditory brainstem of human subjects with ASD are also found in VPA-exposed rodents (human: Kulesza and Mangunay, 2008; Kulesza et al., 2011; Lukose et al., 2015; Mansour and Kulesza, 2021a; rodent: Lukose et al., 2011; Zimmerman et al., 2018; Mansour et al., 2021; Mansour and

*Abbreviations:* ABR, auditory brainstem response; ASD, autism spectrum disorder; CB, calbindin; CI, confidence interval; CR, calretinin; E, embryonic; L, lateral; LVN, lateral vestibular nucleus; M, medial; mc, magnocellular; MVN, medial vestibular nucleus; NT, neurotrace; NHS, normal horse serum; P, postnatal; pc, parvocellular; PBS, phosphate buffered saline; PFA, paraformaldehyde; PVA, primary vestibular afferents; SpN, spinal vestibular nucleus; SupN, superior vestibular nucleus; SOC, superior olivary complex; VEMP, vestibular evoked myogenic potential; VPA, valproic acid.

* Corresponding author at: Department of Anatomy, Lake Erie College of Osteopathic Medicine, 1858 West Grandview Blvd, Erie, PA 16504, United States.
*E-mail address:* rkulesza@lecom.edu (R. Kulesza).

https://doi.org/10.1016/j.brainres.2022.148056
Received 9 March 2022; Accepted 11 August 2022
Available online 17 August 2022

Kulesza, 2021b). Specifically, *in utero* VPA exposure results in significantly fewer neurons throughout the auditory brainstem, reduced axonal projections to the inferior colliculus and medial geniculate, reduced expression of the calcium binding protein calbindin (CB) and calretinin (CR), and abnormal responses to pure tone stimuli (Lukose et al., 2011; Dubiel and Kulesza, 2015; Zimmerman et al., 2018; Mansour et al., 2019; Mansour and Kulesza, 2021b). Further, VPA exposure impacts gross body metrics, neuronal morphology of cerebellar Purkinje cells and performance on certain motor tasks (Main and Kulesza, 2017). In particular, we found that VPA-exposed animals weigh less after weaning, are shorter and have smaller brains and brainstems (Main and Kulesza, 2017, Zimmerman et al., 2018; Mansour et al., 2019) and have significantly delayed eye and ear opening (Zimmerman et al., 2018). In the cerebellum, we found significantly smaller Purkinje cells, reduced expression of the calcium binding protein calbindin (CB) throughout cerebellar lobules I-X, and significantly shorter and less complex Purkinje cell dendrites (Main and Kulesza, 2017). We also frequently found ectopic CB + neurons in the cerebellar granule cell layer (Main and Kulesza, 2017). VPA-exposed animals also had significantly slower righting reflexes, ataxic gate and marked difficulty navigating static beams (Main and Kulesza, 2017). These findings are consistent with previous reports of VPA-induced ataxia and cerebellar dysmorphology (Ingram et al., 2000; Mychasiuk et al., 2012). Notably, VPA appears to have a widespread impact on cerebellar circuitry as *in utero* exposure impacts neuron number and morphology of the deep cerebellar nuclei (Mowery et al., 2015). Vestibular dysfunction and cerebellar abnormalities in human subjects with ASD, together with brainstem changes in VPA-exposed animals lead us to hypothesize that *in utero* VPA exposure impacts vestibular structure and function. We addressed this hypothesis using quantitative morphometrics to examine total number of neurons and cell body morphology in the brainstem vestibular nuclei, immunohistochemistry to examine the distribution of CB + inputs to vestibular nuclei, and a battery of motor tasks and physiological measures to examine vestibular function in an animal model of ASD.

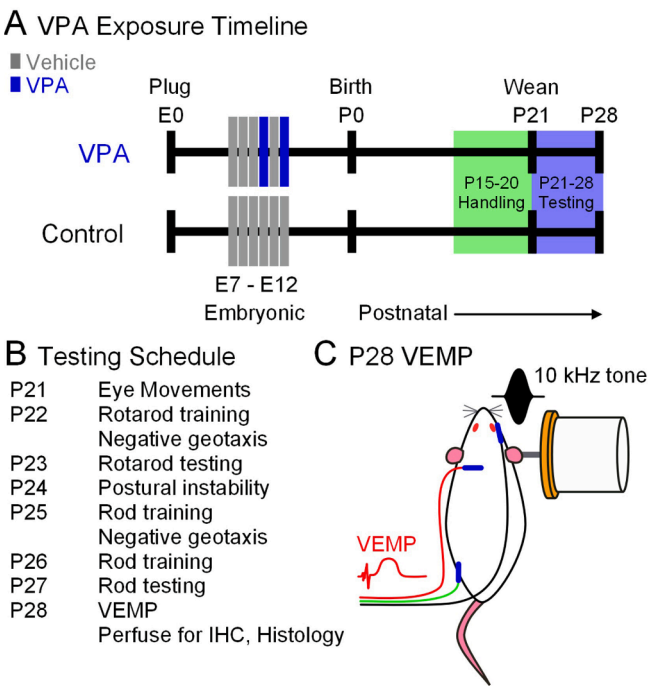


**Fig. 1.** Experimental Paradigm. Shown in A is the schedule for VPA exposure and plan for animal handling and motor testing. Shown in B is the schedule for motor tests. At the conclusion of the vestibular evoked myogenic potential (VEMP) recording on P28, animals were perfused for histology and/or immunohistochemistry (IHC). Shown in C is the electrode array used for recording the VEMP. A 10 kHz tone was played in the right ear and recordings were made from the right paraspinal muscles in the neck (red line). The reference electrode (black) was placed in the right snout and the ground was placed in the left hindlimb (green).

## 2. Results

VPA-exposure resulted in significant morphological changes in the vestibular nuclei. Overall, there were significantly fewer neurons in the vestibular nuclei, although there was no difference in the number of neurons in the medial vestibular nucleus (MVN; control: 21,146 ± 2,022, VPA: 19,780 ± 2,608; p =.13; Fig. 2A-E). There were however significantly fewer neurons in the spinal vestibular nucleus (SpN; control: 12,845 ± 2,922, VPA: 9,428 ± 2,962; t(2.7) = 14, p =.0086), lateral vestibular nucleus (LVN; control: 2,692 ± 501, VPA: 2,505 ± 494; t(1.8) = 14, p =.04) and superior vestibular nucleus (SupN; control: 4,328 ± 1,063, VPA: 2,546 ± 903; t(3.6) = 14, p =.001; Fig. 2A-F). These changes amount to decreases of 27 % of neurons in the SpN and 42 % in the SupN. In the parvocellular (pc) and magnocellular (mc) regions of the MVN and SupN, there was no significant difference in cell body size after VPA exposure (Fig. 2G). However, in the SpN and LV, VPA exposure resulted in significantly larger neuronal cell bodies (Fig. 2b, d, G, H). Specifically, in control animals cell bodies in the SpN measured 161 $\mu m^2$, (CI: 167–189 $\mu m^2$) and in VPA-exposed animals they measured 192 $\mu m^2$ (CI: 203–232 $\mu m^2$; $U(167,179) = 11037$, p <.0001). In control animals cell bodies in the LVN measured 222 $\mu m^2$, (CI: 254–381 $\mu m^2$) and in VPA-exposed animals they measured 341 $\mu m^2$ (CI: 345–472 $\mu m^2$; $U(72,78) = 2141$, p <.005). VPA exposure only impacted the proportions of cell body morphologies in the LVN. In control animals, 81 % of LVN neurons were round/oval and 19 % were stellate. However, in VPA-exposed animals 70 % of LV neurons were round/oval, 25 % were stellate and 5 % were fusiform ($\chi^2$, p =.03).

Since *in utero* VPA exposure results in reduced CB immunolabeling in cerebellar Purkinje cells and auditory brainstem nuclei, we examined the number of CB + puncta on neurons in the vestibular nuclei. In the SupN, CB immunolabeling was too dense in axon profiles and puncta for reliable quantitative analysis. VPA exposure resulted in significantly fewer CB + puncta in the MVN, SpN and LVN (Fig. 3). In control animals, MVN somata were associated with 19 (95 % CI: 16–27) CB + puncta, however MVN somata in VPA-exposed animals had only 8 (95 % CI: 8–11; $U(28,82) = 344$, p <.0001). Likewise, in control animals SpN somata were associated with 17 (95 % CI: 15–23) CB + puncta but in VPA-exposed animals these neurons had only 10 CB + puncta (95 % CI: 7–13; $U(43,51) = 629$, p =.0002). Finally, in control animals LVN somata had 28 (95 % CI: 24–32) CB + puncta and in VPA-exposed animals LVN somata had only 9 CB + puncta (95 % CI: 4–13; $U(38,1000) = 545$, p <.0001).

To examine any possible impact of morphological changes on motor behaviors, we challenged animals with a number of motor tasks. There was no difference in the time animals took to correct posture after being placed in a negative geotaxis position (Fig. 4A). Control animals took 12.25 s (CI: 8.6–15.9 *sec*) and VPA-exposed animals took 11.55 s to correct this posture (CI: 8.9–14.13 *sec*; p =.23). There was no difference in the time animals were able to stay on the accelerated rotarod (control: 203 ± 49 *sec*, VPA: 212 ± 56 *sec*; p =.31; data not shown). In the postural instability test, we found no difference in the positional changes required to elicit limb corrective postures (Fig. 4B). There was no difference between right and left limbs in control (p =.85) or VPA-exposed animals (p =.90) and there was no difference between control and VPA-exposed animals for the right (control: 3.29 ± 0.72 cm, VPA: 3.2 ± 0.67 cm; p =.85) or left upper limb (control: 3.13 ± 0.83 cm, VPA: 3.45 ± 0.83 cm; p =.85; Fig. 4B). However, VPA-exposed animals took significantly longer to traverse the wooden rod (control: 1.55 *sec*, CI: 1.36–3.22; VPA: 2.03, CI: 1.6–5.4; $U(17,16) = 86$, p =.03; Fig. 4C, no challenge). After vestibular challenge, it took VPA-exposed animals almost twice as long to traverse the wooden rod (control: 6.83 *sec*, CI: 1.23–19.2; VPA: 12.32, CI: 9.7–31.77) although this difference was not

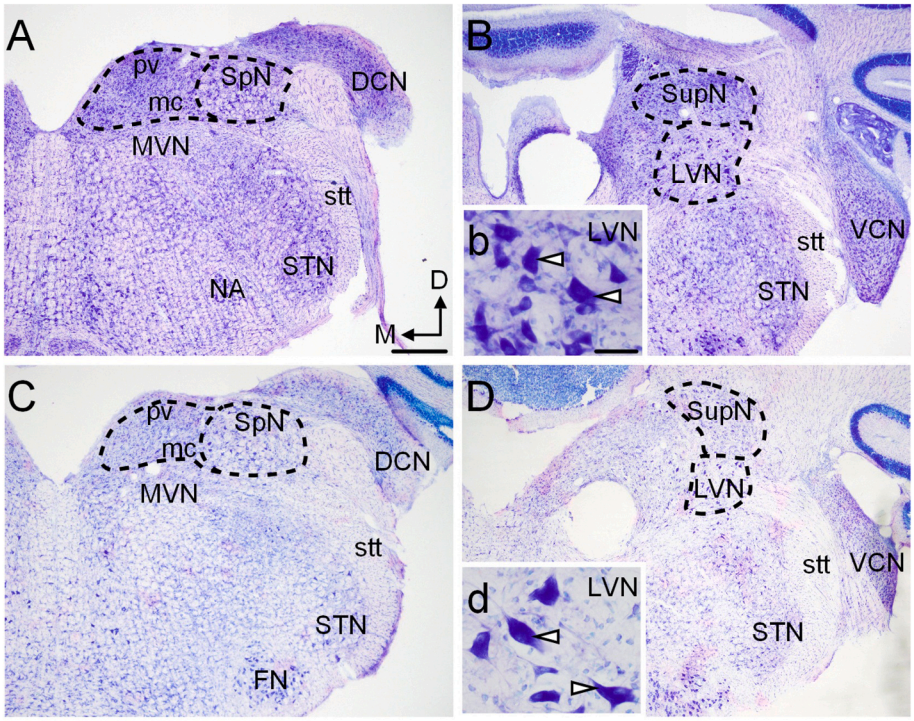


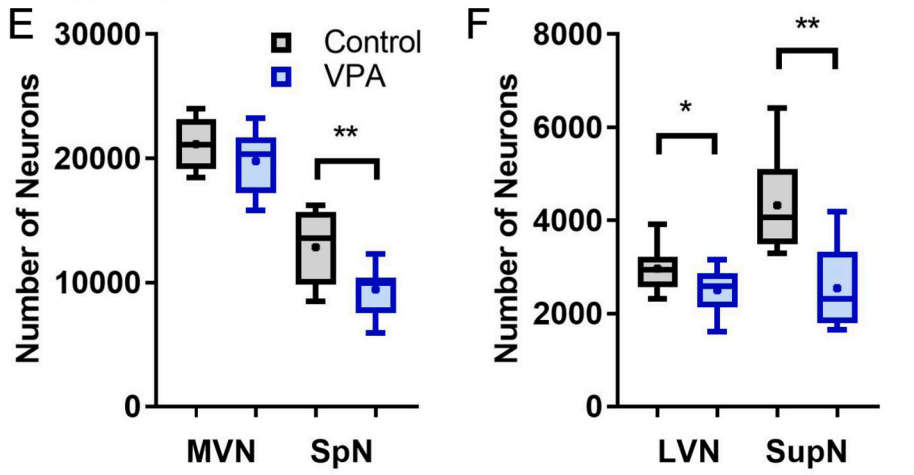


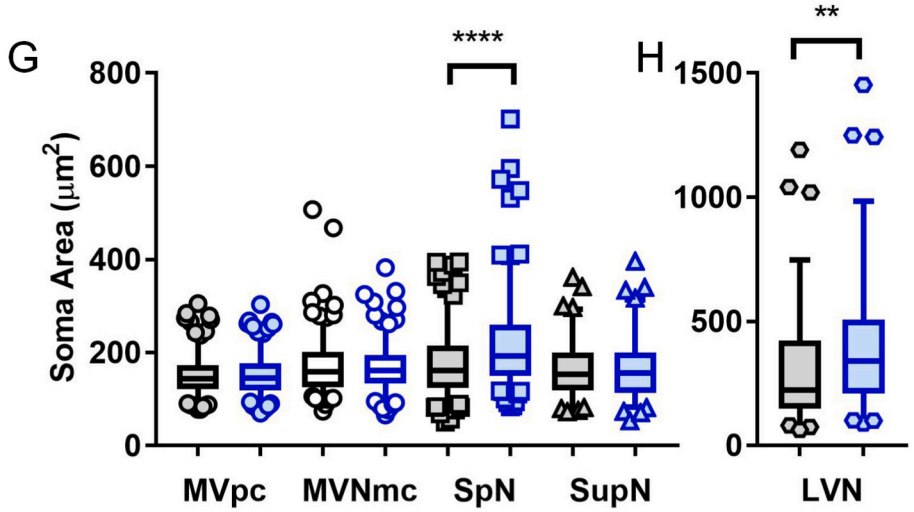


**Fig. 2.** VPA exposure results in dysmorphology in vestibular nuclei. Shown in A and B are different rostrocaudal levels of the brainstem from a control animal. The medial (MVN) and spinal nuclei (SpN) are shown in A (caudal) and the lateral (LVN) and superior nuclei (SupN) are shown in B (rostral). The medial nucleus was divided into parvocellular (pc) and magnocellular regions (mc). Similar regions are shown from a VPA-exposed animal in C (caudal) and D (rostral). The LVN and SupN are noticeably smaller in VPA-exposed animals. High magnification views of the LVN are shown in b (control) and d (VPA). Figures E and F show the total number of neurons in the vestibular nuclei. There are significantly fewer neurons in the SpN, LVN and SupN in VPA-exposed animals. Shown in G and H are the cross-sectional areas of neurons in the vestibular nuclei. In VPA-exposed animals, neurons were significantly larger in the SpN and LVN. Abbreviations: D – dorsal, DCN – dorsal cochlear nucleus, FN – facial nucleus, M – medial, mc – magnocellular, NA – nucleus ambiguous, pv – parvocellular, STN – spinal trigeminal nucleus, stt – spinal trigeminal tract, VCN – ventral cochlear nucleus. Key to symbols: * = p <.05, ** = p <.01, **** = p <.0001. The scale bar in A is equal to 400 μm and applies to A-D; the scale bar in b is equal to 20 μm and applies to d also.

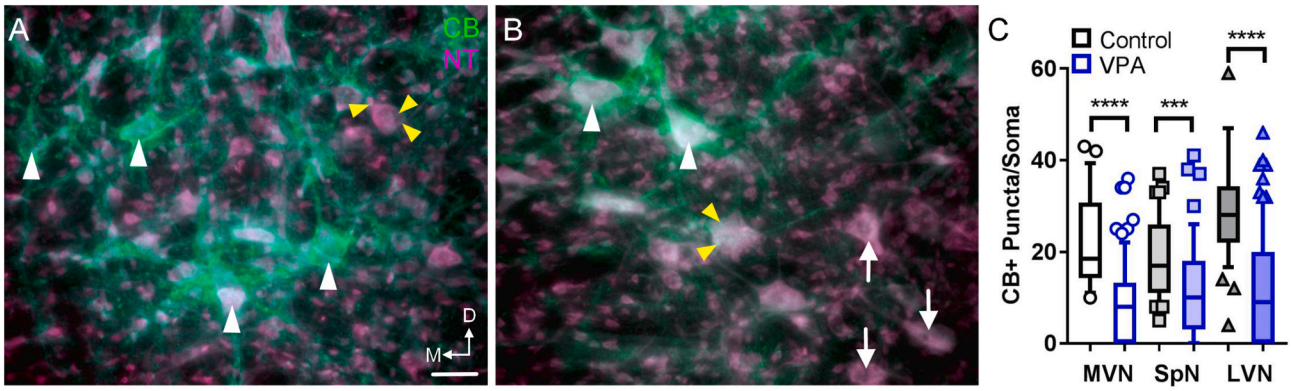


**Fig. 3.** VPA exposure results in fewer CB + puncta. Shown in A and B is CB immunolabeling from the LVN in control (A) and VPA-exposed (B) animals. In control animals, most neuronal cell bodies in the LVN were covered with CB + puncta (white arrowheads), although there were some neurons with few puncta (yellow arrowheads). In VPA-exposed animals, most neurons were associated with CB + puncta however there were significantly fewer than in controls; many neurons did not appear to have any CB + puncta (white arrows). Figure C shows the number of CB + puncta/soma in each of the vestibular nuclei. There were significantly fewer CB + puncta in VPA-exposed animals. Abbreviations: CB – calbindin, D – dorsal, M – medial, NT – neurotrace. Key to symbols: *** = p <.005, **** = p <.0001. The scale bar in A is equal to 20 μm and applies to B also.

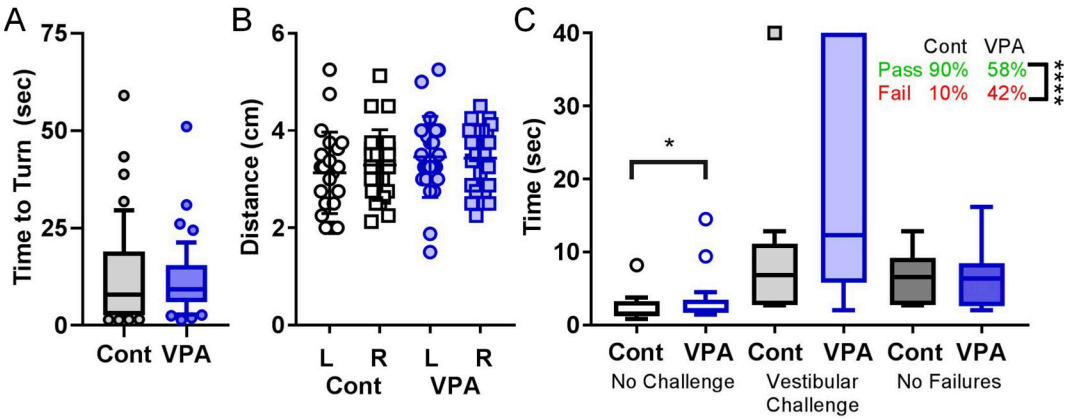


**Fig. 4.** VPA exposure impairs navigation of wooden rods. Figure A shows results of negative geotaxis and time taken to correct negative posture. Figure B shows results from postural instability for both right and left forelimbs. Figure C shows times take to navigate a 25-mm wooden rod. VPA-exposed animals took longer with no challenge and after vestibular challenge, although the latter was not significantly different. The no failures graph shows the vestibular challenge data with only successful attempts (e.g., all failures attempts were removed). VPA-exposed animals had significantly more failed attempts. Abbreviations: L – left, R – right. Key to symbols: * = p <.05, **** = p <.0001.

significant. Removing failed attempts after vestibular challenge revealed no difference between control and VPA-exposed animals on successful attempts (control: 6.55 *sec*, CI: 3.4–9.56; VPA: 6.36, CI: 2.64–11.36; Fig. 4C, no failures). However, there were significantly more failures (42 % of attempts) in VPA-exposed animals compared to controls (10 % of attempts; Fisher's exact test, p <.0001; Fig. 4C). There was no difference in the number of foot slips during routine or vestibular-challenge attempts.

To examine a possible impact of VPA-exposure on physiological measures of vestibular function, we recorded vestibular evoked myogenic potentials (VEMPs) and spontaneous eye movements. VPA exposure resulted in significantly longer latency in the onset of the VEMP (Fig. 5A). In control animals, the onset latency was 6.9 ± 0.49 msec but was 7.6 ± 0.82 msec in VPA-exposed animals (t(2.19) = 14, p =.02; Fig. 5A-B). There was no difference in the positive peak (p1; control: 9.8 ± 1.2 msec, VPA: 9.5 ± 0.42 msec), negative peak (n1; control: 12.58 ± 1.1 msec, VPA: 13.02 ± 1.8 msec), response width (control: 5.6 ± 1.0 msec, VPA: 5.35 ± 2.4 msec) or VEMP amplitude (control: 1.0 ± 0.36 μV, VPA: 1.4 ± 0.87 μV; Fig. 5A-D). Finally, analysis of spontaneous eye movements revealed an impact of VPA-exposure. Specifically, control animals demonstrated only 2.0 ± 1.67 events/10 *sec* (range 0–5, median = 2; Fig. 6A-B). However, VPA-exposed animals had significantly more spontaneous movements (4.42 ± 0.9 events/10 *sec* [range 3–6, median = 4]; t(4.36) = 21, p =.0001; Fig. 6A-B).

## 3. Discussion

### 3.1. General comments

This report constitutes the first study of structural and functional aspects of the vestibular brainstem in an animal model of ASD. Our results reveal hypoplasia and dysmorphology in the vestibular nuclei and impaired motor performance. Within the vestibular nuclei, we found significantly fewer neurons in the SpN, LVN and SupN and larger neuronal cell bodies in the SpN and LVN. Consistent with our finding of fewer neurons, previous work has shown that in animal models of inner ear injury, vestibular dysfunction as indicated by abnormal swimming behaviors, deficient air-righting reflexes and impaired performance on tail hanging tests was linked to lower nuclear volume and decreased neuronal density in vestibular nuclei (Kaiser et al., 2001). Further, we found significantly fewer perisomatic CB + puncta in the MVN, SpN and LVN. Our battery of motor tests revealed that VPA-exposed animals had difficulty navigating wooden rods before and after vestibular challenge, significantly longer latency VEMPs and significantly more spontaneous

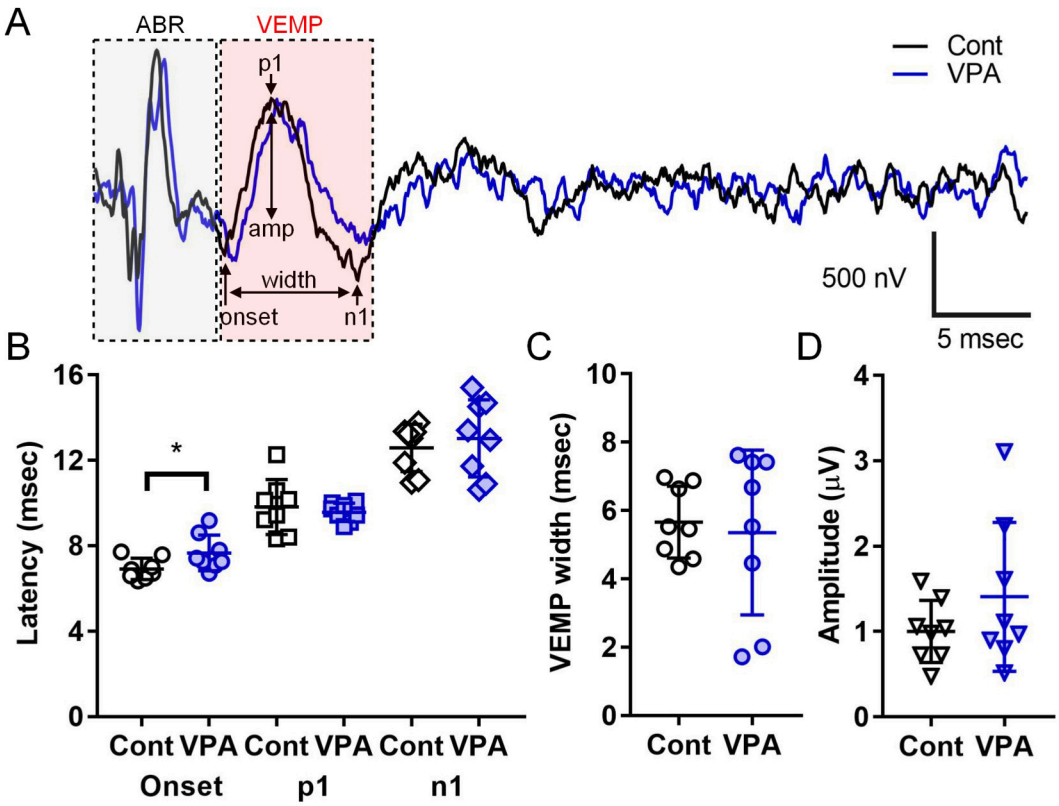


**Fig. 5.** VPA exposure results in longer latency VEMPs. Figure A shows representative VEMP traces from control (black) and VPA-exposed animals (blue). Auditory brainstem responses are indicated in the gray box and VEMPs are indicated in the red box. Figure B shows VEMP onset latencies, peak latency (p1) and negative peak latency (n1). Figure C shows the width of the total VEMP and D shows the amplitude of p1. Key to symbols: * = $p < .05$. Abbreviations: amp – amplitude, auditory brainstem response – ABR, nV – nanovolts, μV - microvolts.

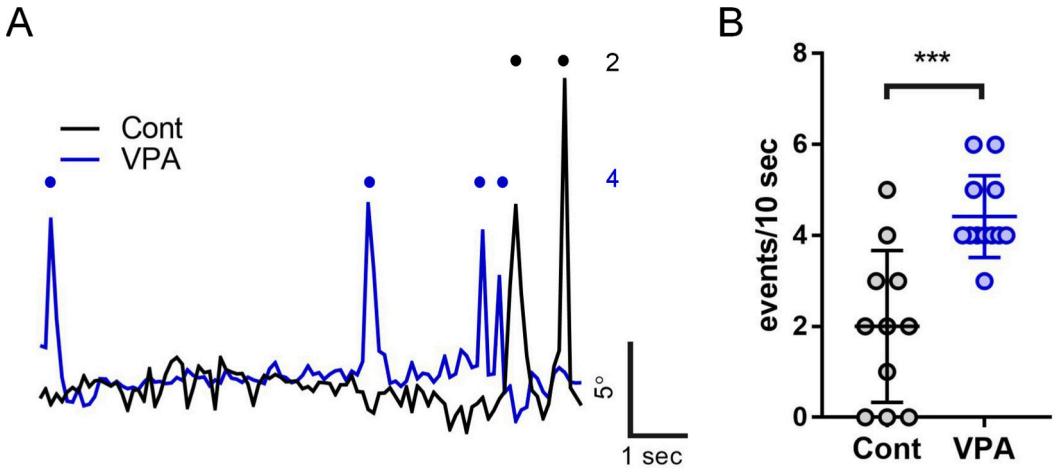


**Fig. 6.** VPA exposure increases spontaneous eye movements. Shown in A are representative tracings of horizontal pupil movements from control (black) and VPA-exposed animals (blue). Each recorded event is indicated by a dot. Shown in B are the number of eye movements (events) per 10 s interval. Key to symbols: *** = $p < .005$.

eye movements. Together with our previous studies of the auditory brainstem and findings of Purkinje cell dysmorphology and ataxia (Main and Kulesza, 2017), we have shown that *in utero* VPA exposure significantly disrupts structure and function of the auditory brainstem (Lukose et al., 2011; Zimmerman et al., 2018; Mansour et al., 2019; Zimmerman et al., 2020; Mansour et al., 2021; Mansour and Kulesza, 2021b), and vestibulocerebellum. The literature provides clear support for involvement of the brainstem and cerebellum in human cases of ASD and several studies document clear neuropathological changes in these regions (Bauman and Kemper, 1985; Courchesne et al., 1988; Hashimoto et al., 1995; Kulesza and Mangunay, 2008; Kulesza et al., 2011; Wegiel et al., 2014a, 2014b; Lukose et al., 2015; Wegiel et al., 2015; Avino et al., 2018; Mansour and Kulesza, 2020). It is important to emphasize that many of the structural changes reported in the auditory brainstem and cerebellum in ASD are reproduced with *in utero* VPA exposure (Lukose et al., 2011; Mychasiuk et al., 2012; Main and Kulesza, 2017; Zimmerman et al., 2018; Mansour et al., 2021; Mansour and Kulesza, 2021a,b). Accordingly, we believe that *in utero* VPA exposure

provides an excellent animal model as a detailed understanding of how brainstem systems and circuits are affected in this condition leading to a better understanding of the neurobiology of ASD, better screening strategies and earlier diagnosis.

### 3.2. VPA exposure results in ataxic gait

The SpN receives its main inputs from primary vestibular afferents (PVA), the cerebellar cortex, and deep cerebellar nuclei; sending axons to the cerebellum and spinal cord, the later via the medial vestibulospinal tract (Brodal, 1978; Haroian, 1984; Matsushita et al., 1995). The LVN receives its main inputs from PVAs, the cerebellar vermis, fastigial nucleus and spinal cord, and projects to the spinal cord as part of the lateral vestibulospinal tract (Shamboul, 1980; Vidal and Sans, 2004). Through descending projections to the spinal cord, both the SpN and LVN function in the control of posture. Interestingly, VPA exposure resulted in fewer but larger neurons in both the SpN and LVN. The functional implication of larger cell bodies is unclear. In the central nucleus of the inferior colliculus of VPA-exposed animals we found significantly fewer neurons, but surviving neurons had larger cells bodies (Mansour et al., 2019). We proposed this increase in soma cross-sectional area results from thicker dendrites with longer and more elaborate dendritic arbors and/or longer/more extensive axonal projections. Abnormally large dendritic arbors might result from impaired pruning during the early postnatal period, and this could lead to abnormal patterns of inputs to the SpN and LVN. Larger cell bodies are required to support longer leading to abnormal patterns of output from the SpN and LVN to the spinal cord (bilateral vs ipsilateral) or aberrant innervation of spinal motor neurons. Further morphological and connectivity studies will be required to clarify this matter in both auditory and vestibular pathways. Our previous study of the cerebellum and motor performance in VPA-exposed animals revealed disorganization of the Purkinje cell layer with occasional ectopic Purkinje cells. These CB + ectopic neurons were most frequently found in lobule X and connectivity of this lobule is consistent with its role in vestibular function (Bernard, 1987). VPA-exposed animals had significantly smaller Purkinje cells across all vermal lobules with the most drastic differences in lobule IV and VI (Main and Kulesza, 2017). We also found drastic changes in the number of CB + Purkinje cells – again all vermal lobules had significantly fewer CB + Purkinje cells. The most drastic change was found in lobule IV – in control animals 91 % of Purkinje cells were CB + but in VPA-exposed animals only 41 % of Purkinje cells were CB +. Cerebellar Purkinje cells in the vermis also had shorter and less complex dendritic arbors. VPA-exposed animals had significantly slower righting reflexes, shorter stride lengths during footprint analysis, difficulty navigating a 25-mm and 12-mm wooden rod with significantly more failed attempts after vestibular challenge and longer latency VEMPS. Consistent with our findings, abnormal VEMPs have been attributed to lesions or dysfunction in PVAs, vestibular nuclei, cerebellum and the medial longitudinal fasciculus (Sheykholeslami et al., 2009; Oh et al., 2016). Based on the role of the cerebellum and vestibular nuclei in motor coordination and posture, we believe the structural changes (i.e., fewer neurons) in these regions are at least partially responsible for slower righting reflexes, gait abnormalities and longer latency VEMPs. However, the impact of VPA on spinal motor neurons and local spinal circuits has not been examined. VPA exposure does result in altered GABAergic neurotransmission (Banerjee et al., 2013; Kumamaru et al., 2014; Olexová et al., 2016; Chau et al., 2017) and auditory hyperexcitability (Dubiel and Kulesza, 2015). Therefore, it is possible the ataxia found in VPA-exposed animals results from a reduction in GABAergic inhibition and subsequent imbalance in excitatory/inhibitory inputs to spinal motor neurons. Consistent with this, VPA exposure results in fewer inhibitory inputs to brainstem oropharyngeal motor neurons (Alhelo and Kulesza, 2021).

### 3.3. VPA exposure results in abnormal eye movements

The SupN receives its main input from PVAs, cerebellar cortex and fastigial nucleus (reviewed in Vidal and Sans, 2004; Halasi et al., 2005). The MVN gets input from PVAs, the cerebellar cortex, fastigial nucleus, spinal cord and direct descending projections from somatosensory cortex (Bernard, 1987; Matsushita et al., 1995; Nishiike et al., 2000). The SupN and MVN both project through the medial longitudinal fasciculus to lower motor neurons controlling eye muscles and together function in stabilization of gaze and posture (Bernard, 1987; Matsushita et al., 1995; Nishiike et al., 2000; Halasi et al., 2005). Again, we found that VPA exposure resulted in fewer neurons in the SupN, fewer CB + inputs to MVN neurons and significantly more spontaneous horizontal eye movements. Given the recognized role of the SupN and MVN in vestibular control of eye movements, we propose the structural changes in these nuclei are at least partially responsible for abnormal eye movements. We interpret the increased number of horizontal spontaneous eye movements as being consistent with ocular nystagmus of central origin. Consistent with this observation, surgical removal of the vestibular ganglion or labyrinth results in altered patterns of input to vestibular nuclei and spontaneous ocular nystagmus in the horizontal plane (Precht, 1986; Li et al., 1995), although these movements return to baseline a few days after the lesion. Children with ASD are 10x more likely to exhibit spontaneous nystagmus (Chang et al., 2021) and we interpret the significant increase in spontaneous eye movements after VPA exposure to be consistent with this finding. Since ocular nystagmus recovers soon after inner ear or vestibular nerve injury, we interpret the findings of nystagmus in subjects ASD and VPA-exposed animals to arise from abnormal patterns of activity in the vestibular nerve, SupN, MVN or cerebellum. We have not examined neuronal number and morphology of lower motor neurons innervating extraocular muscles after VPA exposure. VPA exposure does not impact the number or projections of medial olivocochlear neurons (Mansour and Kulesza, 2021) or number of motor neurons innervating oropharyngeal musculature (Alhelo and Kulesza, 2021). However, VPA exposure does result in an imbalance of excitatory/inhibitory inputs to neurons in the trigeminal motor nucleus, nucleus ambiguous and the hypoglossal nucleus (Alhelo and Kulesza, 2021).

### 3.4. VPA exposure reduces immunolabeling for CB

After VPA exposure there were significantly fewer CB + puncta in the MVN, SpN and LVN. This difference in CB + puncta is exacerbated in the SpN and LVN since these cell bodies are larger after VPA exposure. Previous work in our lab has found that VPA exposure results in significantly fewer CB + neurons in the ventral cochlear nucleus, SOC and dorsal nucleus of the lateral lemniscus (Zimmerman et al., 2018; Mansour et al., 2019) and drastically fewer CB + Purkinje cells (Main and Kulesza, 2017). Not only did we find fewer CB + neurons after VPA exposure, but the few neurons that did have CB immunoreactivity had labeling restricted to the nucleus with little to no cytoplasmic labeling (Zimmerman et al., 2018). Further, VPA exposure results in fewer CR + neurons in the cochlear nucleus and fewer CR + calyceal axons in the trapezoid body and SOC (Zimmerman et al., 2018). However, calyceal axons were labeled by tracer deposits in the trapezoid body and we interpret this to be consistent with reduced brainstem expression of CB and CR. The mechanism for this is unclear but we propose that VPA impacts expression of the genes for CB and CR through its role as a histone deacetylase inhibitor. It is also unclear what impact reduction of CB and CR expression might have on neuronal activity and patterning of action potentials. CB + terminals in the vestibular nuclei arise from cerebellar Purkinje cells, the deep cerebellar nuclei and PVAs (Mehler and Rubertone, 1985; Morris et al., 1988; Bäurle et al., 1998). In rats, PVAs terminate in the MVN, SpN, LVN and SupN (Bäurle et al., 1998). Unilateral labyrinthectomy results in only transient decreases in CB labeling in the cerebellum (Park et al., 2013). Based on our previous

findings, the reduction in the number of CB + inputs in the vestibular nuclei may result from reduced expression of CB and not reduced projections from PVAs and cerebellum.

### 3.5. Does VPA exposure impact other aspects of the vestibular circuit?

Similar to the neurons in the superior olivary complex (SOC), the majority of neurons in the vestibular nuclei originate on E11-15 (Altman and Bayer, 1980). Our previous work revealed that VPA exposure results in significantly fewer neurons in the SOC (Lukose et al., 2011; Zimmerman et al., 2018) and reduced ascending axonal projections to the midbrain and thalamus (Mansour et al., 2019; Zimmerman et al., 2020). Accordingly, we hypothesize that VPA exposure results in significantly reduced axonal projections from the vestibular nuclei to the cerebellum and spinal cord and that these changes would be most prominent in the SpN and LVN. Even though we have identified numerous changes in both the auditory and vestibular brainstem pathways, we have not yet examined the sensory epithelium in the inner ear or morphological features or projections of neurons in the spiral and vestibular ganglia. It is possible that *in utero* VPA exposure impairs hair cell development and/or disrupts projections and number of spiral and vestibular ganglia.

### 3.6. Summary and conclusions

Our previous work in human subjects with ASD and VPA-exposed animals reveals significant and consistent disruption of auditory brainstem structure and function. Several recent studies provide evidence for ataxia and abnormal eye movements in ASD and our study of VPA-exposed animals show significant dysmorphology in brainstem vestibular nuclei and cerebellum. This work provides a basis for further study of vestibular nuclei in ASD. We hope that better understanding of the involvement of the auditory and vestibular brainstem in ASD will lead to development of a battery of simple, non-invasive screening test for early diagnosis and treatment.

## 4. Experimental procedures

### 4.1. VPA exposure

All handling and physiological recordings were approved by the LECOM Institutional Animal Care and Use Committee (protocols #20–02 and 21–03) and conducted in accordance with the National Institute of Health Guide for the Care and Use of Laboratory Animals. Sprague–Dawley rats were maintained on a 12 h light/dark cycle with *ad libitum* access to food and water. *In utero* exposure to VPA was performed as previously described (Fig. 1A; Main and Kulesza 2017; Zimmerman et al. 2018; Mansour et al. 2019; Zimmerman et al., 2020; Mansour et al., 2021, Mansour and Kulesza, 2021). Briefly, dams were fed 3.1 g of peanut butter on embryonic days (E) 7–12. On E10 and E12, dams in the VPA group were fed peanut butter mixed with 800 mg/kg of VPA (Fig. 1A). Control animals were fed peanut butter meals according to the same schedule but without VPA. Pups were delivered without interference and litters were not culled. On postnatal day (P) 21, litters were weaned and only male pups were included in the study since gender-specific effects of VPA exposure are established (Schneider et al. 2008; Mowery et al., 2015). Pups used in this study were randomly selected from each litter – we worked under the assumption that all male pups were equally afflicted by VPA exposure; our previous reports are consistent with this strategy (Main and Kulesza 2017; Zimmerman et al. 2018; Mansour et al. 2019; Zimmerman et al., 2020; Mansour et al., 2021; Mansour and Kulesza, 2021).

### 4.2. Motor testing & evoked potentials

To ensure animals undergoing motor testing were acclimated to researchers and the testing environment, animals were handled for 3–5 min from P15 through P20 (Fig. 1A-B). The schedule for motor testing is shown in Fig. 1B. On *P*21, animals were lightly restrained by hand, and a ScopeAround ear camera was positioned 2–3 cm from the animal's right eye and spontaneous eye movements were recorded for 60 s and saved as an MP4 file (640x480 pixels @ 20 frames/*sec*; see below). These video files were imported into EyeLoop (https://github.com/simonarvin/eyeloop#data; Arvin et al., 2021) and eye movements were tracked using the corneal reflection feature. From the video recordings, we isolated stable epochs of at least 10 s for analysis. Eye movement events were classified as rapid deflections at least 25 % above the baseline. On P22 and P25, animals underwent negative geotaxis testing. Briefly, animals were placed nose-down on a wooden board set at an angle of 45° from horizontal. We measured the time it took animals to correct the negative (nose-down) posture (i.e., turning 180° to nose-up position); this was measured three times on each day. On *P*23, animals underwent a 5-minute training session on a rotarod (Med Associates, Inc). On P24, animals were subjected to postural instability testing. Animals were hand restrained with their right forelimb held against their torso and their left forelimb positioned on a table. Animals were slowly moved forward by the researcher, and we measured the forward displacement required for the animal to reposition their left forelimb. Measurements were taken from video recordings of each session. This was measured over three repetitions for each forelimb. On P25 and P26, animals were trained to navigate an elevated (15° Incline) 600 mm long, 25 mm wide wooden beam. Each training session required the animals to navigate the entire length of the beam three times. On P27, we measure how long it took for animals to navigate the wooden beam. We then subjected animals to a vestibular challenge – animals were placed in a plastic cup attached to a drill and spun at a rate of 3 Hz for 20 s. Animals were then placed on the wooden beam and timed to navigate the full distance. All navigation events were video recorded – observations of foot slips (i.e., paws coming off the rod after contact) were made from the videos. Animals that fell from the rod during an attempted navigation were assigned a time of 40 s (4x the longest successful navigation). On P28, animals underwent recording of a vestibular evoked myogenic potential (VEMP; Fig. 1C; Yang and Young, 2005; Day et al., 2007; Sheykholeslami et al., 2009). Animals were initially anesthetized with 4–5 % isoflurane in $O_2$ (1.2 L/min); when animals were unresponsive the isoflurane was lowered to 3 % and they were moved to a sound attenuated chamber. Animals were positioned in a flexed posture to stretch the paraspinal muscles; the recording electrode penetrated the cervical paraspinal musculature near the spinous processes and extended ~ 1 cm from medial to lateral (perpendicular to the muscle fibers; Fig. 1C, red line). The reference electrode was placed in the right snout (Fig. 1C, black line) and the ground electrode was placed subcutaneously in the left hindlimb (Fig. 1C, green line). Impedance for the recording and reference electrodes were equal to or less than 1kΩ. A 10 kHz tone was played at 70 dB into the right external auditory meatus through a closed-field electrostatic speaker (Tucker Davis Technologies) with a 3 cm tube. The tone was driven by a RZ6 Bioacoustics System for 512 repetitions. Sound-evoked activity from the recording electrode was collected on a low-impedance head stage (Tucker Davis Technologies; RA4L1), preamplified and digitized on a RA16D Medusa preamp and sent to a RZ6 processor over fiber-optic cable. Signals were filtered (100–5000 Hz, with a 60 Hz notch filter) and averaged using BioSigRZ software. Latencies and amplitudes were determined by visually placing cursors in the BioSig trace window.

### 4.3. Sectioning and histology

Animals used for morphology (control, n = 4 [3 litters]; VPA, n = 4 [3 litters]) were anesthetized with an overdose of vaporized isoflurane on P28. When animals were unresponsive to toe pinch, they were perfused through the ascending aorta with normal saline followed by 4 % paraformaldehyde (PFA) in phosphate buffered saline (PBS; pH 7.4; fixative). Brains were dissected from the skull and the right side of the

brain was marked with a register pin. Brains were stored in 4 % PFA-PBS (at 4 °C) for at least 24 h. Brains were cryoprotected in 30 % sucrose at room temperature for at least 24 h and sectioned in the coronal plane on a freezing-stage microtome at a thickness of 50 μm. Every third tissue section was collected serially into PBS and mounted from cresyl gelatin onto glass slides in caudal-to-rostral sequence. Sections were stained for Nïssl substance with Giemsa (Sigma-Aldrich, St Louis, MO), dehydrated through ascending alcohols, cleared and coverslipped with Permount (ThermoFisher Scientific, Waltham, MA).

### 4.4. Neuronal morphology

The vestibular nuclei were studied with an Olympus BX45 microscope and neuronal cell bodies were traced by an observer blinded to animal group using a 40x objective (final magnification of 680x). We followed the delineation of the vestibular nuclei (medial vestibular nucleus – MVN, parvocellular and magnocellular; spinal vestibular nucleus – SpN; lateral vestibular nucleus – LVN; superior vestibular nucleus - SupN) provided in Paxinos and Watson (2007). Tracings of neuron cell bodies were digitized and quantified using ImageJ (1.52; Reuden et al., 2017). An index of circularity was calculated for each cell body profile using the following equation:

$$\text{Circularity} = \left[4p^{*}\text{Area}/\text{Perimeter}^{2}\right]$$

Classification of cell body shape was made according to objective, morphometric measures. Cell body profiles that had a circularity measure greater than 0.6 were classified as round/oval; those with a major axis/minor axis greater than 3 were classified as fusiform. All remaining profiles were classified as stellate. We have previously correlated these criteria with distinct cell body morphologies in the rodent auditory brainstem (Mansour et al., 2019).

### 4.5. Estimates of neuronal number

The total number of neurons in each of the vestibular nuclei were estimated in control and VPA-exposed animals. Neuronal packing density was calculated by counting neuronal profiles in an evenly spaced series of sections through each nucleus. These counts were corrected using Konigsmark's (1970) formula (for recent application in auditory brainstem see rat: Mansour et al., 2019a; Mansour et al., 2021; human: Mansour et al., 2019b) to account for profile splitting (rearranged):

$$N = n(t/t + 2a)$$

N is the estimated number of neurons, n is the number of counted neuronal profiles, t is section thickness and "a" is the square root of $r^2 - (k/2)^2$. In calculation of "a", we used the nucleolus correction (Konigsmark, 1970). Here, r is the average radius of nucleoli and k is the diameter of nucleoli fragments. The density of neuronal profiles was calculated by dividing the corrected counts (N) by the tissue volume from which they were counted. The number of neurons in each region was finally estimated by multiplying the calculated neuronal density by the estimated volume of the nucleus (Thompson and Brenowitz, 2005). The method has produced neuronal estimates statistically similar to the optical dissector in the auditory brainstem (Kulesza et al., 2002; Kulesza, 2007; Zimmerman et al., 2018; Mansour et al., 2019a; Mansour et al., 2021).

### 4.6. Immunohistochemistry

Free-floating brainstem sections were rinsed in PBS, then blocked in 1 % normal horse serum (NHS; AbCam), 0.5 % triton X in PBS for 1 h. Sections were incubated in rabbit anti-CB (1:1000 with 1 % NHS; AbCam, catalog #: ab11426) overnight, rinsed in PBS and incubated for 2 h in goat anti-rabbit Dylight 488 (1:100; Vector Labs). Sections were rinsed, counterstained with Neurotrace Red (NT; ThermoFisher Scientific), mounted onto glass slides, dried and coverslipped with Entellan (Millipore Sigma). Images of NT and CB labeling were overlaid in ImageJ; we counted the number of CB + punctate profiles adjacent to NT labeled cell bodies.

### 4.7. Statistics

Descriptive statistics were generated for all datasets using GraphPad Prism 7.03 (GraphPad Software, La Jolla, CA) and tested against a normal distribution using the D'Agostino & Pearson omnibus normality test. If data fit a normal distribution, comparisons were conducted using parametric tests (*t* test or ANOVA) and results are presented as mean ± standard deviation. If data failed to fit the normal distribution, comparisons were conducted using non-parametric tests and are presented as the median with the 95 % confidence interval (CI) of the median. The distribution of cell body shape was examined using the Chi-square test. Differences were considered statistically significant if p values were $< 0.05$.

## Declaration of Competing Interest

The authors declare that they have no known competing financial interests or personal relationships that could have appeared to influence the work reported in this paper.

## Acknowledgements

The authors would like to thank the Lake Erie Consortium for Osteopathic Medical Training for funding and Luke Smith for assistance with Python and running EyeLoop.

## References

Alhelo, H., Kulesza, R.J., 2021. Brainstem motor neuron dysmorphology and excitatory/inhibitory imbalance in an animal model of autism. Folia Morphol. (Warsz).
Allen, D.A., 1988. Autistic spectrum disorders: clinical presentation in preschool children. J. Child Neurol. 3 (Suppl), S48–S56.
Altman, J., Bayer, S.A., 1980. Development of the brain stem in the rat. III. Thymidine-radiographic study of the time of origin of neurons of the vestibular and auditory nuclei of the upper medulla. J. Comp. Neurol. 194 (4), 877–904.
American Psychiatric Association. Diagnostic and statistical manual of mental disorders (5th ed.). Washington, DC: Author. 2013.
Arvin, S., Rasmussen, R.N., Yonehara, K., 2021. EyeLoop: An Open-Source System for High-Speed, Closed-Loop Eye-Tracking. Front. Cell. Neurosci. 9 (15), 779628.
Avino, T.A., Barger, N., Vargas, M.V., Carlson, E.L., Amaral, D.G., Bauman, M.D., Schumann, C.M., 2018. Neuron numbers increase in the human amygdala from birth to adulthood, but not in autism. Proc. Natl. Acad. Sci. U. S. A. 115 (14), 3710–3715.
Banerjee, A., García-Oscos, F., Roychowdhury, S., Galindo, L.C., Hall, S., Kilgard, M.P., Atzori, M., 2013. Impairment of cortical GABAergic synaptic transmission in an environmental rat model of autism. Int. J. Neuropsychopharmacol. 16 (6), 1309–1318.
Bauman, M., Kemper, T.L., 1985. Histoanatomic observations of the brain in early infantile autism. Neurology. 35 (6), 866–874.
Bäurle, J., Vogten, H., Grüsser-Cornehls, U., 1998. Course and targets of the calbindin D-28k subpopulation of primary vestibular afferents. J. Comp. Neurol. 402 (1), 111–128.
Bernard, J.-F., 1987. Topographical organization of olivocerebellar and corticonuclear connections in the rat: An WGA-HRP study. I. Lobules IX, X and the flocculus. J. Comp. Neurol. 263 (2), 241–258.
Brodal, A., 1978. The cranial nerves: Anatomy and anatomico-clinical correlations. Blackwell Scientific Publ.
Bromley, R.L., Mawer, G.E., Briggs, M., Cheyne, C., Clayton-Smith, J., Garcia-Finana, M., Kneen, R., Lucas, S.B., Shallcross, R., Baker, G.A., Baker, G., Briggs, M., Bromley, R., Clayton-Smith, J., Dixon, P., Fryer, A., Gummery, A., Kneen, R., Kerr, L., Lucas, S., Mawer, G., Shallcross, R., 2013. Liverpool and Manchester Neurodevelopment Group. The prevalence of neurodevelopmental disorders in children prenatally exposed to antiepileptic drugs. J. Neurol. Neurosurg. Psychiatry 84 (6), 637–643.
Centers for Disease Control and Prevention. Autism and developmental disabilities monitoring (ADDM) network. 2022, January 11. https://www.cdc.gov/ncbddd/autism/addm.html.
Chang, M.Y., Doppee, D., Yu, F., Perez, C., Coleman, A.L., Pineles, S.L., 2021. Prevalence of ophthalmologic diagnoses in children with autism spectrum disorder using the optum dataset: APopulation-based study. Am. J. Ophthalmol. 221, 147–153.
Chau, D.K., Choi, A.Y., Yang, W., Leung, W.N., Chan, C.W., 2017. Downregulation of glutamatergic and GABAergic proteins in valproric acid associated social impairment during adolescence in mice. Behav. Brain Res. 1 (316), 255–260.

Christensen, J., Grønborg, T.K., Sørensen, M.J., Schendel, D., Parner, E.T., Pedersen, L.H., Vestergaard, M., 2013. Prenatal valproate exposure and risk of autism spectrum disorders and childhood autism. JAMA 309 (16), 1696–1703.
Courchesne, E., Yeung-Courchesne, R., Press, G.A., Hesselink, J.R., Jernigan, T.L., 1988. Hypoplasia of cerebellar vermal lobules VI and VII in autism. N. Engl. J. Med. 318 (21), 1349–1354.
Day, A.S., Lue, J.H., Yang, T.H., et al., 2007. Effect of intratympanic application of aminoglycosides on click-evoked myogenic potentials in Guinea pigs. Ear Hear 28, 18–25.
Dubiel A, Kulesza RJ. Prenatal valproic acid exposure disrupts tonotopic c-Fos expression in the rat brainstem. Neuroscience. 2015 Dec 17;311:349-61. doi: 10.1016/j.neuroscience.2015.10.043. Epub 2015 Oct 28. Erratum in: Neuroscience. 2016 Jun 2;324:510. Corrected and republished in: Neuroscience. 2016 Jun 2;324:511-23.
Halasi, G., Bácskai, T., Matesz, C., 2005. Connections of the superior vestibular nucleus with the oculomotor and red nuclei in the rat: an electron microscopic study. Brain Res. Bull. 66 (4–6), 532–535.
Haroian, A.J., 1984. Fastigial afferent projections in a rat: An HRP study. Anat. Rec. 208, 71A.
Hashimoto, T., Tayama, M., Murakawa, K., Yoshimoto, T., Miyazaki, M., Harada, M., Kuroda, Y., 1995. Development of the brainstem and cerebellum in autistic patients. J. Autism Dev. Disord. 25 (1), 1–18.
Ingram, J.L., Peckham, S.M., Tisdale, B., Rodier, P.M., 2000. Prenatal exposure of rats to valproic acid reproduces the cerebellar anomalies associated with autism. Neurotoxicol. Teratol. 22 (3), 319–324.
Kaiser, A., Fedrowitz, M., Ebert, U., Zimmermann, E., Hedrich, H.J., Wedekind, D., Löscher, W., 2001. Auditory and vestibular defects in the circling (ci2) rat mutant. Eur. J. Neurosci. 14 (7), 1129–1142.
Konigsmark, B., 1970. Methods for the counting of neurons, in contemporary research method in neuroanatomy. Springer, New York, pp. 315–380.
Koren, G., et al., 2006. Major malformations with valproic acid. Can. Fam. Physician 52 (4), 441–442.
Kulesza, R.J., 2007. Cytoarchitecture of the human superior olivary complex: medial and lateral superior olive. Hear. Res. 225 (1-2), 80–90.
Kulesza, R.J., Mangunay, K., 2008. Morphological features of the medial superior olive in autism. Brain Res. 20 (1200), 132–137.
Kulesza, R.J., Viñuela, A., Saldaña, E., Berrebi, A.S., 2002. Unbiased stereological estimates of neuron number in subcortical auditory nuclei of the rat. Hear. Res. 168 (1-2), 12–24.
Kulesza Jr, R.J., Lukose, R., Stevens, L.V., 2011. Malformation of the human superior olive in autistic spectrum disorders. Brain Res. 7 (1367), 360–371.
Kumamaru, E., Egashira, Y., Takenaka, R., Takamori, S., 2014. Valproic acid selectively suppresses the formation of inhibitory synapses in cultured cortical neurons. Neurosci. Lett. 21 (569), 142–147.
Li, H., Godfrey, D.A., Rubin, A.M., 1995. Comparison of surgeries for removal of primary vestibular inputs: a combined anatomical and behavioral study in rats. Laryngoscope. 105 (4 Pt 1), 417–424.
Lukose, R., Schmidt, E., Wolski Jr., T.P., Murawski, N.J., Kulesza Jr., R.J., 2011. Malformation of the superior olivary complex in an animal model of autism. Brain Res. 1398, 102–112.
Lukose, R., Beebe, K., Kulesza Jr., R.J., 2015. Organization of the human superior olivary complex in 15q duplication syndromes and autism spectrum disorders. Neuroscience 12 (286), 216–230.
Mabunga, D.F., Gonzales, E.L., Kim, J.W., Kim, K.C., Shin, C.Y., 2015. Exploring the Validity of Valproic Acid Animal Model of Autism. Exp. Neurobiol. 24 (4), 285–300.
Main, S.L., Kulesza, R.J., 2017. Repeated prenatal exposure to valproic acid results in cerebellar hypoplasia and ataxia. Neuroscience 6 (340), 34–47.
Mansour, Y., Kulesza, R., 2020. Three dimensional reconstructions of the superior olivary complex from children with autism spectrum disorder. Hear. Res. 393, 107974.
Mansour, Y., Kulesza, R., 2021a. Distribution of glutamatergic and glycinergic inputs onto human auditory coincidence detector neurons. Neuroscience 1 (468), 75–87.
Mansour, Y., Burchell, A., Kulesza, R.J., 2021. Central Auditory and Vestibular Dysfunction Are Key Features of Autism Spectrum Disorder. Front. Integr. Neurosci. 29 (15), 743561.
Mansour, Y., Kulesza, R.J., 2021b. The untouchable ventral nucleus of the trapezoid body: preservation of a nucleus in an animal model of autism spectrum disorder. Front. Integr. Neurosci. 15, 730439.
Mansour, Y., Mangold, S., Chosky, D., Kulesza, R.J., 2019. Auditory midbrain hypoplasia and dysmorphology after prenatal valproic acid exposure. Neuroscience 1 (396), 79–93.
Matsushita, M., Gao, X., Yaginuma, H., 1995. Spinovestibular projections in the rat, with particular reference to projections from the central cervical nucleus to the lateral vestibular nucleus. J. Comp. Neurol. 361 (2), 334–344.
Mehler, W.R., Rubertone, J.A., 1985. Anatomy of the vestibular nucleus complex. In: Paxinos, G. (Ed.), The Rat Nervous System. Vol. 2. Hindbrain and Spinal Cord. Academic Press, New York, pp. 185–219.
Moore, S.J., Turnpenny, P., Quinn, A., Glover, S., Lloyd, D.J., Montgomery, T., Dean, J. C., 2000. A clinical study of 57 children with fetal anticonvulsant syndromes. J. Med. Genet. 37 (7), 489–497.
Morris, R.J., Beech, J.N., Heizmann, C.W., 1988. Two distinct phases and mechanisms of axonal growth shown by primary vestibular fibres in the brain, demonstrated by parvalbumin immunohistochemistry. Neuroscience 27, 571–596.
Mowery, T.M., Wilson, S.M., Kostylev, P.V., Dina, B., Buchholz, J.B., Prieto, A.L., Garraghty, P.E., 2015. Embryological exposure to valproic acid disrupts morphology of the deep cerebellar nuclei in a sexually dimorphic way. Int. J. Dev. Neurosci. 40, 15–23.
Mychasiuk, R., Richards, S., Nakahashi, A., Kolb, B., Gibb, R., 2012. Effects of rat prenatal exposure to valproic acid on behaviour and neuro-anatomy. Dev. Neurosci. 34 (2–3), 268–276.
Nishiike, S., Guldin, W.O., Baurle, J., 2000. Corticofugal connections between the cerebral cortex and the vestibular nuclei in the rat. J. Comp. Neurol. 420 (3), 363–372.
Oh, S.Y., Kim, H.J., Kim, J.S., 2016. Vestibular-evoked myogenic potentials in central vestibular disorders. J. Neurol. 263 (2), 210–220.
Olexová, L., Štefánik, P., Kršková, L., 2016. Increased anxiety-like behaviour and altered GABAergic system in the amygdala and cerebellum of VPA rats - An animal model of autism. Neurosci. Lett. 26 (629), 9–14.
Ornitz, E.M., 1969. Disorders of perception common to early infantile autism and schizophrenia. Compr. Psychiatry 10, 259–274.
Park, B.R., Choi, M.A., Hong, S.M., 2013. Temporal changes of calbindin expression in the nodulus following unilateral labyrinthectomy in rats. Neurosci. Lett. 25 (555), 47–50.
Paxinos, G., Watson, C., 2007. The rat brain in stereotaxic coordinates. Academic Press, London.
Precht, W., 1986. Recovery of some vestibuloocular and vestibulospinal functions following unilateral labyrinthectomy. Prog. Brain Res. 64, 381–389.
Rasalam, A.D., Hailey, H., Williams, J.H., Moore, S.J., Turnpenny, P.D., Lloyd, D.J., Dean, J.C., 2005. Characteristics of fetal anticonvulsant syndrome associated autistic disorder. Dev. Med. Child Neurol. 47 (8), 551–555.
Rodier, P.M., Ingram, J.L., Tisdale, B., Nelson, S., Romano, J., 1996. Embryological origin for autism: developmental anomalies of the cranial nerve motor nuclei. J. Comp. Neurol. 370 (2), 247–261.
Schneider, T., Roman, A., Basta-Kaim, A., Kubera, M., Budziszewska, B., Schneider, K., Przewłocki, R., 2008. Gender-specific behavioral and immunological alterations in an animal model of autism induced by prenatal exposure to valproic acid. Psychoneuroendocrinology. 33 (6), 728–740.
Shamboul, K.M., 1980. Lumbosacral predominance of vestibulospinal fiber projection in the rat. J. Comp. Neurol. 192, 519–530.
Sheykholeslami, K., Megerian, C.A., Zheng, Q.Y., 2009. Vestibular evoked myogenic potentials in normal mice and Phex mice with spontaneous endolymphatic hydrops. Otol. Neurotol. 30 (4), 535–544.
Smith, A., Storti, S., Lukose, R., Kulesza Jr., R.J., 2019. Structural and Functional Aberrations of the Auditory Brainstem in Autism Spectrum Disorder. J. Am. Osteopath. Assoc. 119 (1), 41–50.
Thompson, C.K., Brenowitz, E.A., 2005. Seasonal change in neuron size and spacing but not neuronal recruitment in a basal ganglia nucleus in the avian song control system. J. Comp. Neurol. 481 (3), 276–283.
Vidal, P.P., Sans, A., 2004. Vestibular System. In: The Rat Nervous System, 3rd ed. Elsevier, San Diego, pp. 964–995.
Wegiel, J., Flory, M., Kuchna, I., Nowicki, K., Ma, S.Y., Imaki, H., Wegiel, J., Cohen, I.L., London, E., Wisniewski, T., Brown, W.T., 2014a. Stereological study of the neuronal number and volume of 38 brain subdivisions of subjects diagnosed with autism reveals significant alterations restricted to the striatum, amygdala and cerebellum. Acta Neuropathol. Commun. 18 (2), 141.
Wegiel, J., Flory, M., Kuchna, I., Nowicki, K., Ma, S.Y., Imaki, H., Wegiel, J., Cohen, I.L., London, E., Brown, W.T., Wisniewski, T., 2014b. Brain-region-specific alterations of the trajectories of neuronal volume growth throughout the lifespan in autism. Acta Neuropathol. Commun. 10 (2), 28.
Wegiel, J., Flory, M., Kuchna, I., Nowicki, K., Ma, S.Y., Imaki, H., Wegiel, J., Frackowiak, J., Kolecka, B.M., Wierzba-Bobrowicz, T., London, E., Wisniewski, T., Hof, P.R., Brown, W.T., 2015. Neuronal nucleus and cytoplasm volume deficit in children with autism and volume increase in adolescents and adults. Acta Neuropathol. Commun. 17 (3), 2.
Williams, G., King, J., Cunningham, M., Stephan, M., Kerr, B., Hersh, J.H., 2001. Fetal valproate syndrome and autism: additional evidence of an association. Dev. Med. Child Neurol. 43 (3), 202–206.
Wing, L., 1997. The autistic spectrum. Lancet. 1997 Dec 13;350(9093):1761-6. doi: 10.1016/S0140-6736(97)09218-0. PMID: 9413479.
Yang TH, Young YH. Click-evoked myogenic potentials recorded on alert guinea pigs. Hear Res 2005;205:277Y83.
Zhao, H., Wang, Q., Yan, T., Zhang, Y., Xu, H.J., Yu, H.P., Tu, Z., Guo, X., Jiang, Y.H., Li, X.J., Zhou, H., Zhang, Y.Q., 2019. Maternal valproic acid exposure leads to neurogenesis defects and autism-like behaviors in non-human primates. Transl. Psychiatry 9 (1), 267.
Zimmerman, R., Patel, R., Smith, A., Pasos, J., Kulesza Jr., R.J., 2018. Repeated Prenatal Exposure to Valproic Acid Results in Auditory Brainstem Hypoplasia and Reduced Calcium Binding Protein Immunolabeling. Neuroscience 1 (377), 53–68.
Zimmerman, R., Smith, A., Fech, T., Mansour, Y., Kulesza Jr., R.J., 2020. In utero exposure to valproic acid disrupts ascending projections to the central nucleus of the inferior colliculus from the auditory brainstem. Exp. Brain Res. 238 (3), 551–563.